Three-dimensional crystal growth. I. Linear analysis and self-similar evolution

V. Cristini* and J. Lowengrub†

School of Mathematics, and Department of Chemical Engineering and Materials Science, University of Minnesota, Minneapolis, MN 55455

(May 9, 2001)

Abstract

In this paper, Part I of our study, we revisit the linear analysis [1–3] of the quasi-steady diffusional evolution of growing crystals in 3-D. We focus on a perturbed spherical solid crystal growing in an undercooled liquid with isotropic surface tension and interface kinetics. We investigate the relation between the far-field flux of temperature and undercooling in the far-field. In 3-D, the flux scales with the undercooling and with the instantaneous size of the crystal; this behavior is qualitatively different from 2-D, where there is no dependence on the size. As a consequence of this peculiarity, we demonstrate using linear analysis that in 3-D there exist critical conditions of flux at which self-similar evolution occurs. This leads to nonspherical, shape-invariant growing crystals. The critical flux increases with increasing wave-number of the perturbation, and separates regimes of stable and unstable growth, where stable growth implies that the perturbation decays with

*E-mail: cristini@cems.umn.edu

†Corresponding author: School of Mathematics, University of Minnesota, 206 Church Street, Minneapolis, MN 55455. Tel: (612) 625 0753; Fax: (612) 626 2017; E-mail: lowengrb@math.umn.edu

respect to the underlying sphere. The interfacial kinetics have a strong stabilizing effect [2,3], which is explored in detail here. These results demonstrate that the classical Mullins-Sekerka [1] instability, that arises in the presence of constant undercooling, can be suppressed by maintaining near-critical flux conditions. Correspondingly, there is little creation of unstable modes during growth and unstable growth is very constrained or completely eliminated. Near-critical flux conditions can be achieved by appropriately varying the undercooling in time; thus this work has important implications for shape control in processing applications. Experiments are currently being designed (by Stefano Guido and coworkers [4] at the University of Naples) to test this possibility. Moreover, in Part II [5] of our study, we will investigate the nonlinear evolution using adaptive boundary-integral simulations.

Keywords: A1. Crystal morphology; A1. Diffusion; A1. Morphological stability; A2. Growth from melt; A2. Single crystal growth.

Pacs: 81.10.A; 64.70.D

I. INTRODUCTION

The case of quasi-steady crystal growth is a fundamental problem both in phase transitions and in diffusion dominated growth (e.g., see the review paper by Fried and other papers in [6]). The growth of a spherical germ from a supercooled melt or supersaturated solution (with isotropic surface tension) was first analyzed by Mullins and Sekerka [1]. It was found that a growing sphere is linearly unstable to large-wavelength perturbations. Moreover, as the sphere becomes larger, smaller wavelengths successively become unstable. This provides a heuristic explanation for the dendritic and highly complex shapes typically observed in freezing processes in nature (e.g. snowflakes). Later, Coriell and Parker [2,3] extended the study to finite interfacial kinetics, which was found to have a stabilizing effect, while leaving

the qualitative behavior unchanged.

In this paper, Part I of our study, we revisit the linear analysis [1–3] of the quasi-steady diffusional evolution of growing crystals in 3-D. We focus on a perturbed spherical solid crystal growing in an undercooled liquid with isotropic surface tension and interface kinetics. We exploit the relation between temperature flux and undercooling to directly control shape evolution during growth. In 3-D, the flux scales with the undercooling and with the instantaneous size of the crystal, $J_0 \sim |T^\infty| R$ using characteristic values; this behavior is qualitatively different from 2-D, where there is no dependence on the size. Because of this peculiarity, we find that in 3-D there exist critical conditions of flux J_l, that depends on the wavenumber l of the perturbation, so that, corresponding to a weakly time-dependent flux $J \approx J_l$, self-similar evolution occurs, leading to nonspherical, shape-invariant growing crystals. The evolution is identically self-similar for constant (critical) flux and no kinetics. In the presence of kinetics, the evolution is self-similar at long times for constant flux; identically self-similar evolution may be achieved using the weakly time-dependent flux. The critical flux increases as $J_l \sim l^2$ at large l, and separates regimes of stable and unstable growth. The interfacial kinetics have a strong stabilizing effect [2,3], which is explored in detail here. Analogous self-similar evolution has been recently found in tumor growth [7].

These results reveal that the Mullins-Sekerka [1] instability, that arises in the presence of constant undercooling ($J_0 \sim R$), can be suppressed by maintaining flux conditions close to critical. Correspondingly, there is little creation of unstable modes during growth and unstable growth is very constrained or completely eliminated. Near-critical flux conditions can be achieved by appropriately varying the undercooling in time. Note that Mullins and Sekerka recognized the possibility of stable growth paths obtained by varying the undercooling (see Fig. 1 in [1]). In Part II of our study, we demonstrate using boundary-integral simulations that the linear relation between flux and undercooling, that is presented in this paper, holds quantitatively even in the nonlinear regime. This result has important implications for shape control in processing applications; shape control may be achieved by varying the undercooling in time to approximate near-critical conditions. Experiments are currently

being designed (by Stefano Guido and coworkers [4] at the University of Naples) to test this possibility.

In §II, the equations that govern the problem are formulated. The linear analysis is presented in §III. Conclusions, work in progress and directions of future work are given in §IV.

II. GOVERNING EQUATIONS

A. Dimensional formulation

Consider the quasi-steady [1] diffusional evolution of temperature T in the unbounded multiphase domain $\mathbf{R}^3 = \Omega_1 \cup \Omega_2$, where an interfacial surface Σ divides the solid phase 1 from the (infinite) liquid phase 2. The dimensional system is

$$0 = \nabla^2 T_i, \qquad \text{in } \Omega_i, \quad i = 1, 2, \tag{2.1}$$

where temperature $T_i = T_i(\mathbf{x}, t)$, where $\mathbf{x}$ is position in space and t is time. The Gibbs-Thomson boundary conditions on the moving boundary $\Sigma \equiv \partial\Omega_1$ are [2]

$$(T_1)_\Sigma = (T_2)_\Sigma = T_{\rm PH} \cdot \left(1 - \frac{\gamma\ \kappa}{\mathcal{L}}\right) - \mu^{-1} V \tag{2.2}$$

where $T_{\rm PH}$ is the phase change temperature for a flat interface, γ is the (uniform) surface tension, $\mathcal{L}$ is the latent heat per unit volume (the density is taken to be equal in the two phases and constant), κ is the total curvature of Σ ($\kappa = 2$ on the unit sphere), μ is the (uniform) kinetic coefficient (a linear kinetic relation is assumed), and V is the normal velocity of Σ:

$$V = \mathbf{n} \cdot (K_1 \nabla T_1 - K_2 \nabla T_2)_\Sigma\,, \tag{2.3}$$

where $\mathbf{n}$ is the normal vector to Σ directed into Ω_2 and $K_{1,2} = k_{1,2}/\mathcal{L}$, where $k_{1,2}$ are the heat conductivities.

In the far-field, we prescribe the flux J of T into the system: $J = -(4\pi)^{-1} \int_{\Sigma^\infty} \mathbf{n} \cdot \nabla T \, \mathrm{d}\Sigma^\infty$, where Σ^∞ is an arbitrary boundary in the far-field, and $\mathbf{n}$ is its outward normal. Using the quasi-steady diffusion equation (2.1) in Ω_1 and Ω_2, it can be easily shown that this definition of J is equivalent to

$$J = (4\pi)^{-1} \int_\Sigma V \, \mathrm{d}\Sigma, \tag{2.4}$$

which also gives the rate of volume growth (the numeric factor 4π is introduced to simplify the formulas in §III). This far-field condition is different from that taken in the classical Mullins-Sekerka (MS) problem [1] in which equation (2.4) is replaced by

$$\lim_{|\mathbf{x}| \to \infty} T_2(\mathbf{x}, t) = T^\infty, \tag{2.5}$$

where T^∞ is the temperature in the far field.

In this physical system, the diffusion times $\tau_{D_{1,2}} = R_0^2/D_{1,2}$, where R_0 is the initial equivalent radius of the crystal and $D_{1,2}$ are the diffusion coefficents, are small compared to all other time scales. Thus, there are three relevant time scales: the surface tension relaxation time τ_γ, the kinetic attachment time τ_μ and the growth time τ_∞, which are given by

$$\tau_\gamma = \frac{R_0^2}{K_2 \Delta T_\gamma}, \qquad \tau_\mu = \frac{R_0}{\mu \Delta T_\gamma}, \qquad \tau_\infty = \frac{R_0^2}{K_2 \Delta T_0^\infty}. \tag{2.6}$$

where $\Delta T_\gamma = \gamma T_{\mathrm{PH}}/(\mathcal{L} R_0)$ is the characteristic decrease in phase change temperature with respect to a flat interface, and $\Delta T_0^\infty = T_{\mathrm{PH}} - T_0^\infty$ is the initial undercooling (T_0^∞ is the initial temperature in the far-field).

From equation (2.4), with motion on the time scale τ_∞ given by (2.6), we obtain the following relation between the characteristic flux $J_0 = R_0^3/\tau_\infty$ and undercooling ΔT_0^∞:

$$\frac{J_0}{K_2 \Delta T_0^\infty} \sim R_0. \tag{2.7}$$

Eq. (2.7) reveals that in three dimensions, the relative magnitude of the flux and undercooling scales with the characteristic size of the system R_0. We note that this result is *different*

than the analogous result in two dimensions, where $J_0 = R_0^2/\tau_\infty$, and thus, from (2.6), $J_0 \sim K_2 \Delta T_0^\infty$, independently of system size. The scaling (2.7), peculiar to three dimensions, gives rise to a very different behavior than in two dimensions [8,9], and to the possibility of self-similar evolution under constant-flux conditions, as will be exploited in this paper.

B. Dimensionless Formulation

We nondimensionalize the physical variables as

$$t' = t/\tau_\gamma, \quad |\mathbf{x}'| = |\mathbf{x}|/R_0, \quad T' = \frac{T - T_{\rm PH}}{\Delta T_\gamma}. \tag{2.8}$$

The nondimensional flux J' is given by

$$J' = Ca\ J/J_0, \tag{2.9}$$

where Ca is a dimensionless capillary number that rescales flux is

$$Ca = \tau_\gamma/\tau_\infty, \tag{2.10}$$

which characterizes the relative importance of surface tension and undercooling.

In dimensionless form, equations (2.1)–(2.5) become, after dropping all the primes,

$$\begin{aligned} 0 &= \nabla^2 T_i \qquad \text{in } \Omega_i,\ i = 1, 2, \\ (T_1)_\Sigma = (T_2)_\Sigma &= -\kappa - \epsilon\ V, \\ V &= \mathbf{n} \cdot (k\ \nabla T_1 - \nabla T_2)_\Sigma\,, \\ &\begin{cases} J = (4\pi)^{-1} \displaystyle\int_\Sigma V \,\mathrm{d}\Sigma, \quad \text{or} \\ \\ \displaystyle\lim_{|\mathbf{x}| \to \infty} T_2(\mathbf{x}, t) = T^\infty. \end{cases} \end{aligned} \tag{2.11}$$

In both the far-field flux and MS formulations, there are three dimensionless parameters[1]—the kinetic coefficient ϵ and the ratio of conductivities k, given by

[1]Actually, there is a fourth dimensionless parameter ρ_1/ρ_2 which we have taken to be equal to 1 by setting the densities $\rho_1 = \rho_2$.

$$\epsilon = \tau_\mu/\tau_\gamma, \qquad k = k_1/k_2, \tag{2.12}$$

and either J or T^∞. We note that ϵ and Ca may also be related to ratios of temperatures: $\epsilon = \Delta T_\mu/\Delta T_\gamma$ and $Ca = \Delta T_0^\infty/\Delta T_\gamma$, where the temperature decrease associated with kinetics is $\Delta T_\mu = R_0/(\mu\tau_\gamma)$.

As an example of physical system, for *water*, typically [10] $\gamma = 7\cdot 10^{-2}\mathrm{N/m}$, $T_{\mathrm{PH}} \approx 273\mathrm{K}$, $\mathcal{L} = 335\cdot 10^6\mathrm{J/m^3}$, thus, for a crystal of radius $R_0 = 1\mu\mathrm{m}$, $\Delta T_\gamma \approx 0.057\mathrm{K}$. A characteristic value of $k_2 = 0.6\mathrm{J/(msK)}$, which gives $K_2 = 1.8\cdot 10^{-9}\mathrm{m^2/(sK)}$, and $\tau_\gamma \approx 10^{-2}\mathrm{s}$. Data for kinetic coefficients have a wide variation [3,10].

III. LINEAR ANALYSIS

We consider the linearized evolution of a sphere of radius R perturbed by a spherical harmonic $Y_{l,m}$

$$r_\Sigma(\theta,\phi,t) = R(t) + \delta(t)\ Y_{l,m}(\theta,\phi), \tag{3.1}$$

where θ is the polar angle (measured from $\hat{\mathbf{z}}$ to $\hat{\mathbf{r}}$) and ϕ is the azimuthal angle (measured from $\hat{\mathbf{x}}$ to the projection of $\hat{\mathbf{r}}$ in the x-y plane)[2].

To begin, expand equation (2.11)d in powers of δ, and use the expansion of the normal velocity $V = \mathrm{d}R/\mathrm{d}t + O(\delta/R)$, to obtain the flux

$$J(t) = R^2\ \frac{\mathrm{d}R}{\mathrm{d}t} + O\left(\delta/R\right)^2. \tag{3.2}$$

Taking J constant in time, yields the simple result in Eq. (3.13) using $R(0) = 1$ from the nondimensionalization: $R = (1 + 3J\ t)^{\frac{1}{3}}$. On the other hand, Coriell & Parker [3] showed that

$$T^\infty(t) = -(R+\epsilon)\ \frac{\mathrm{d}R}{\mathrm{d}t} - 2/R + O\left(\delta/R\right)^2. \tag{3.3}$$

---

[2]By the hat, we denote unit vectors. The vectors $\hat{\mathbf{x}}$, $\hat{\mathbf{y}}$ and $\hat{\mathbf{z}}$ define the cartesian coordinate directions. The vectors $\hat{\mathbf{r}}$, $\hat{\theta}$ and $\hat{\phi}$ define the spherical coordinate directions.

Consequently from Eqs. (3.2) and (3.3), the flux and T^∞ are related by

$$J = \frac{-1}{1+\epsilon/R}\,(T^\infty R + 2) + O(\delta/R)^2. \tag{3.4}$$

Thus, $J > 0$ and growth occurs when $-T^\infty > 2/R$ which is the total curvature of the sphere. When $R \gg 1$, the flux $J \sim -T^\infty R$, as suggested by the scaling analysis in Eq. (2.7). The result for 2-D, analogous to (3.4), is $J = -\left(T^\infty + 1\right) / \left(1 + \epsilon/R\right) + O(\delta/R)^2$.

A. Stability of Perturbation

By expanding the system of equations (2.11) in powers of δ, and matching linear terms, we find that the linear evolution of the perturbation is governed by:

$$\delta^{-1}\,\frac{\mathrm{d}\delta}{\mathrm{d}t} = \frac{l-1}{R^3}\,\frac{J - \left(1+\bar{k}\;l\right)(l+2)}{1+\left(1+\bar{k}\;l\right)\epsilon/R}, \tag{3.5}$$

where $\bar{k} = 1 + k$. Thus, the morphology of the perturbed sphere results from competition between the destabilizing effect of volume flux J and the stabilizing effects of surface energy (in dimensionless form, given by the negative term in the numerator) and interface kinetics (in the denominator). Since ϵ appears only in the ratio ϵ/R, kinetics becomes less important in the evolution as the sphere grows. Also observe that the parameter m does not play a role in the linear analysis.

Characterizing the evolution of the perturbation, relative to the underlying evolution of the sphere, one considers the ratio δ/R, that describes the shape of the crystal. We define three cases:

1. Stable evolution: $\delta/R \to 0$ as $t \to \infty$.
2. Unstable evolution: $\delta/R \to \infty$ as $t \to \infty$.
3. Bounded evolution: $0 < |\delta/R| < \infty$ for $t \geq 0$.

Note that Coriell & Parker [3] called case 1 absolute stability and the special case $\frac{\mathrm{d}}{\mathrm{d}t}\,(\delta/R) = 0$ relative stability. Using Eqs. (3.2) and (3.5), we obtain the growth rate

$$(\delta/R)^{-1}\ \frac{\mathrm{d}}{\mathrm{d}t}\,(\delta/R) = \frac{1}{R^3}\ \frac{(J-J_l)(l-2) - J\cdot(1+\bar{k}\ l)\ \epsilon/R}{1+(1+\bar{k}\ l)\ \epsilon/R}, \tag{3.6}$$

where a critical flux J_l is given by

$$J_l = \frac{(l+2)(l-1)(1+\bar{k}\ l)}{l-2}. \tag{3.7}$$

Clearly, if $0 \le J \le J_l$ and $t \ge 0$, then the growth rate $(\delta/R)^{-1}\,\frac{\mathrm{d}}{\mathrm{d}t}\,(\delta/R) \le 0$. Thus, the evolution is either stable or bounded, and $\delta/R \le \delta_0$, where $\delta_0 = \delta(0)$ and $R(0) = 1$. For example, if the flux $J = 0$ (the volume of the precipitate is conserved), then from Eq. (3.2), we obtain $R = 1$ identically and from Eq. (3.5) the evolution is stable with the perturbation decaying exponentially in time:

$$\delta^{-1}\ \frac{\mathrm{d}\delta}{\mathrm{d}t} = -\frac{(l+2)(l-1)(1+\bar{k}\ l)}{1+(1+\bar{k}\ l)\ \epsilon}. \tag{3.8}$$

On the other hand, taking $J = J_l$ leads to bounded (but not stable) evolution, as demonstrated in §§III B–III D, where this case will be explored in detail.

If $J > J_l$, then the evolution may be either unstable or bounded. Taking

$$J = J_l\ \frac{l-2}{l-2-(1+\bar{k}\ l)\ \epsilon/R}, \tag{3.9}$$

the growth rate (3.6) vanishes and the evolution is self-similar: $\delta/R = \delta_0$ identically. Note that this special value of flux (3.9) is greater than J_l for $\epsilon > 0$, and depends on the instantaneous size of the growing crystal; note also that, if $\epsilon = 0$, then taking $J = J_l$ yields self-similar evolution. When $J =$ constant, $J < J_l$ yields stable evolution, and $J > J_l$ yields unstable evolution.

Next, let us characterize the maximum growth rate $(\delta/R)^{-1}\,\frac{\mathrm{d}}{\mathrm{d}t}\,(\delta/R)$. We determine the flux that makes the l-th mode have the largest growth rate. This is important if the initial condition contains a superposition of spherical harmonics since the fastest growing harmonic tends to dominate the shape. Maximizing the growth rate in Eq. (3.6) with respect to l, we find that the corresponding flux J is given by

$$J = \frac{1+2l+\bar{k}\cdot(3l^2+2l-2) + \Big(1+2l+\bar{k}\ l\cdot\Big(2\bar{k}\ l^2 + l\cdot(4+\bar{k})+2\Big)\Big)\ \epsilon/R}{1+(1+\bar{k})\ \epsilon/R}. \tag{3.10}$$

In the limit $\epsilon/R \to 0$, this reduces to

$$J_l^* = 1 + 2l + \bar{k} \cdot \left(3l^2 + 2l - 2\right). \tag{3.11}$$

Therefore, in this limit, the maximum growth rate is achieved with the constant flux J_l^*. Note that for $l > 3$, $J_l^* > J_l$. In figure 1, the flux J from Eq. (3.10) is plotted versus R/ϵ with $\bar{k} = 2$ for several values of l (solid curves). Corresponding to each mode l, the mode q that marks the upper bound of the band of unstable modes is shown (for $\epsilon/R = 0$). This mode q is found by equating $J_l^* = J_q$, with J_q obtained from Eq. (3.7) with l replaced by q. This means that mode q has zero growth rate ($q-1$ is the largest unstable mode) when the flux in the system is equal to J_l^*. For large l, we obtain $q \approx 3^{\frac{1}{2}} l$.

The effect of kinetics is seen in figure 1 through the variation of J with R, which is most prominent for large l since the nondimensional kinetic parameter ϵ is multiplied by $(1 + \bar{k}\ l)$ in the growth rate in Eq. (3.6). To demonstrate the difference between constant flux and temperature, dotted lines are plotted for two (constant) values of flux and a dashed curve is plotted which corresponds to the flux obtained from Eq. (3.4) for a constant T^∞. When, during the evolution, a dotted line or dashed curve intersects a solid one, the corresponding mode l is the mode with largest growth rate. Thus, when the flux is constant no unstable modes are created as the precipitate grows unless the kinetic effect is large, i.e. $(1+\bar{k}\, l)\, \epsilon \sim R$. In contrast, when T^∞ is constant, the number of unstable modes increases without bound as the precipitate grows.

B. Special Cases

Let us now consider two special cases: constant J and constant T^∞. If J is constant, then Eq. (3.6) can be integrated to yield the growth factor

$$\frac{\delta/\delta_0}{R} = R^{(l-2)(1-J_l/J)} \cdot \left(\frac{1 + (1 + \bar{k}\ l)\ \epsilon/R}{1 + (1 + \bar{k}\ l)\ \epsilon}\right)^{1+(l-1)(1-J_l/J)}, \tag{3.12}$$

where

$$R = (1 + 3J\ t)^{\frac{1}{3}}, \tag{3.13}$$

from Eq. (3.2). Alternatively, if T^∞ is constant, then

$$\frac{\delta/\delta_0}{R} = R^{l-2} \cdot \left(\frac{1 + (1 + \bar{k}\ l)\ \epsilon/R}{1 + (1 + \bar{k}\ l)\ \epsilon}\right)^{(l-1)(1+\alpha_1)} \left(\frac{T^\infty + 2/R}{T^\infty + 2}\right)^{-\alpha_2}, \tag{3.14}$$

where the exponents are given by

$$\alpha_1 = \frac{\bar{k}\ l \cdot (l+2)}{2 - \epsilon\ T^\infty \cdot (1 + \bar{k}\ l)}, \quad \alpha_2 = \frac{(l-1)(l+2)(1 + \bar{k}\ l)(2 - \epsilon\ T^\infty)}{2(2 - \epsilon\ T^\infty \cdot (1 + \bar{k}\ l))}, \tag{3.15}$$

and the radius R is given implicitly by

$$t = -\frac{1}{2T^\infty}\left(R^2 - 1\right) - \frac{2 - \epsilon\ T^\infty}{{T^\infty}^3}\left(-T^\infty \cdot (R-1) + 2\log\frac{2 + R\ T^\infty}{2 + T^\infty}\right), \tag{3.16}$$

from Eq. (3.3). At long times, Eqs. (3.12) – (3.16) reduce to

$$\frac{\delta/\delta_0}{R} \approx \frac{R^{(l-2)(1-J_l/J)}}{\left(1 + (1 + \bar{k}\ l)\ \epsilon\right)^{1+(l-1)(1-J_l/J)}}, \qquad R \approx (3J\ t)^{\frac{1}{3}} \qquad \text{(constant } J\text{)}; \tag{3.17}$$

$$\frac{\delta/\delta_0}{R} \approx \frac{R^{(l-2)} \cdot (1 + 2/T^\infty)^{\alpha_2}}{\left(1 + (1 + \bar{k}\ l)\ \epsilon\right)^{(l-1)(1+\alpha_1)}}, \qquad R \approx (-2T^\infty t)^{\frac{1}{2}} \qquad \text{(constant } T^\infty\text{)}. \tag{3.18}$$

The difference in scaling, $R \sim t^{\frac{1}{2}}$ for constant undercooling, and $R \sim t^{\frac{1}{3}}$ for constant flux, reflects the difference between the classical theories of growth [1] and coarsening [11,12].

In the constant flux case, Eq. (3.12) shows that for $J < J_l$ the evolution is stable, for $J > J_l$ unstable, and for $J = J_l$ bounded. In the constant temperature case, Eq. (3.14) shows that the linear solutions always become unstable. These behaviors are illustrated in figure 2 where the growth factor $(\delta/\delta_0)/R$ is plotted as a function of R. We have set $l = 3$, $k = 1$ and $\epsilon = 0.1$. The solid and dashed curves correspond to constant J and T^∞ respectively. At time $t = 0$, the J and T^∞ are related by the formula (3.4): $J = 7.27$ corresponds to $T^\infty = -10$, $J = 70$ to $T^\infty = -79$, and $J = \infty$ to $T^\infty = -\infty$. Eq. (3.12) shows that when $J = J_l$, the evolution tends to be self-similar as $t \to \infty$ and

$$\lim_{t\to\infty} \frac{\delta/\delta_0}{R} = \left(1 + (1 + \bar{k}\ l)\ \epsilon\right)^{-1}, \tag{3.19}$$

which is marked by the open circle in the figure. Note that the limiting shape depends on ϵ. It is easily shown, from (3.12)–(3.13) with $J = J_l$, that there is a kinetic transient on a time scale $O\left(J_l^{-1}\right)$ that may reduce the perturbation by an amount $O(\epsilon)$ (cf. Eq. (3.19)). If $J \ll J_l$ and constant, there is a transient on the time scale $O\left(J_l^{-1} \cdot (l-2)^{-1}\right)$ in which the shape relaxes to a sphere ($\delta = 0$). In the constant temperature case, equations (3.14) and (3.16) reveal that there is a transient on the time scale $O\left(|T^\infty|^{-1}\right)$ in which the perturbation may be reduced, both in the presence and in the absence of kinetics. If $J \gg J_l$ and constant, then the growth factor $\sim R^{l-2}$ and the shape evolves on a time scale $O\left(J^{-1}\right)$. If $|T^\infty| \gg 1$ and constant, then as in the flux case, the growth factor $\sim R^{l-2}$, on the time scale $O\left(|T^\infty|^{-1}\right)$. The dot-dashed curves in figure 2 have slope equal to $l-2$ corresponding to the limiting behavior $(\delta/\delta_0)/R \sim R^{l-2}$ that holds if either T^∞ is constant or $J \gg J_l$ and constant. Finally, the dotted curve in figure 2 has slope equal to $(1 - J_3/J)$.

C. The Effect of Kinetics

We next examine the effect of kinetics in more detail. Rewriting Eq. (3.9), we obtain the radius R_l^* at which the growth rate is equal to zero:

$$R_l^* = \epsilon \, \frac{1 + \bar{k}\, l}{l-2} \left(1 - J_l/J\right)^{-1}, \tag{3.20}$$

which diverges as $J \to J_l$. In the case of constant flux or temperature, R_l^* corresponds to a minimum in the growth factor $(\delta/\delta_0)/R$. For constant flux, the associated time scale for evolution to this minimum is $t_l^* \sim (1 - J_l/J)^{-3}$. This shows that the evolution of precipitates in near-critical conditions is slow: $t_l^* \to \infty$ as $J \to J_l$. If this scaling also holds in the presence of nonlinearity, it may be used to determine a critical nonlinear flux J_l^{NL} by extrapolating numerical results for $J \approx J_l^{\mathrm{NL}}$.

Another measure of the kinetics may be obtained by considering the value R_l^{**} such that for $R \geq R_l^{**}$ the growth factor $(\delta/\delta_0)/R \geq 1$ indicating that perturbations grow relative to the underlying sphere. In the constant flux case, we obtain the implicit relation

$$\frac{R_l^{**} - (R_l^{**})^{\alpha_3}}{(1 + \bar{k}\ l)\ ((R_l^{**})^{\alpha_3} - 1)} = \epsilon, \tag{3.21}$$

where

$$\alpha_3 = 1 - \frac{(l-2)(1 - J_l/J)}{l + (l-1)J_l/J}. \tag{3.22}$$

For the constant temperature case, an analogous implicit relation can be derived from (3.14). In figure 3, the dependence of R_l^* and R_l^{**} on ϵ for several values of l is illustrated. The dot-dashed, dashed and solid curves correspond to $l = \infty$, $l = 4$ and $l = 3$ respectively. The flux $J = 1.1 J_l$ and the horizontal line marks $\epsilon = 0.1$. Note that the curves start at the same point ($R_l^* = R_l^{**} = 1$) with the upper curve being R_l^*. Observe that for a given ϵ, $R_l^* < R_l^{**}$ and the difference $R_l^{**} - R_l^*$ increases with decreasing l. For $l = 4$ and $\epsilon = 0.1$, for example, $R_4^* \approx 5$ while $R_4^{**} \approx 90$. As $J \to J_l$, the growth factor $(\delta/\delta_0)/R \leq 1$ and $R_l^* \to \infty$. The limit $J \to \infty$ yields upper bounds, for each l and ϵ, that are qualitatively similar to the curves plotted in figure 3. We note that the dependence of R_l^* upon ϵ and l was previously investigated by Coriell & Parker [3] in the constant temperature case.

D. Self-similar Evolution

In section III A, we remarked that the evolution may be self-similar if the flux J is given by Eq. (3.9). In addition, self-similar behavior also occurs, as $t \to \infty$, if $J = J_l$. This is seen from Eq. (3.12), which reduces to

$$\frac{\delta/\delta_0}{R} = \frac{1 + (1 + \bar{k}\ l)\ \epsilon/R}{1 + (1 + \bar{k}\ l)\ \epsilon}, \tag{3.23}$$

where $R = (1 + 3J_l\, t)^{\frac{1}{3}}$. Thus, in the limit as $t \to \infty$ ($R \to \infty$), this yields Eq. (3.19). Therefore, for each l and m, linear theory predicts that there is a nontrivial limiting precipitate shape given by

$$\frac{r_\Sigma}{R} \to 1 + \frac{\delta_0}{1 + (1 + \bar{k}\ l)\ \epsilon}\ Y_{l,m}(\theta, \phi), \quad \text{as} \quad t \to \infty. \tag{3.24}$$

Observe that the effect of ϵ and l is to reduce the size of the limiting perturbation. And, in the absence of kinetics, the initial perturbation is preserved.

There are also other, more general conditions under which self-similar behavior is obtained at long times. For example, by integrating the growth rate $(\delta/R)^{-1}\frac{\mathrm{d}}{\mathrm{d}t}(\delta/R)$, we obtain the condition

$$\lim_{R\to\infty}\left|\int_1^R (1 - J_l/J(\zeta))\ \frac{\mathrm{d}\zeta}{\zeta}\right| < \infty \tag{3.25}$$

(where ζ is the integration variable), which, if satisfied, ensures that there is a limiting, non-spherical shape. This can be achieved if, for instance, the flux satisfies

$$(1 - J_l/J(R)) = O\left(R^{-\nu}\right), \tag{3.26}$$

for any $\nu > 0$.

IV. CONCLUSIONS

We revisited the linear analysis of the quasi-steady diffusional evolution of growing crystals in 3-D. We focused on a solid perturbed spherical crystal growing in an undercooled liquid with isotropic surface tension and interface kinetics. We exploited the relation between temperature flux and undercooling to use flux as a shape-control parameter. Because of the peculiar scaling of flux with the instantaneous size of the crystal and with the far-field temperature, $J \sim |T^\infty|\, R$, we found that in 3-D there exist nearly constant critical flux conditions $J \approx J_l$ at which destabilizing flux and stabilizing surface tension effects balance identically. This leads to self-similar evolution during growth, and to nonspherical, shape-invariant crystals. This result reveals that the Mullins-Sekerka [1] instability, that arises under constant-temperature (increasing-flux) conditions, may be suppressed by appropriately decreasing the far-field temperature in time: $|T^\infty| \sim R^{-1}J_l$, to maintain desired near-critical flux conditions during growth.

The critical flux $J_l \sim l^2$ at large wavenumbers, and separates regimes of stable (decaying to zero with respect to the underlying sphere) and unstable growth of perturbations. In

contrast to the classical Mullins-Sekerka instability, unstable growth is very constrained in 3-D under near-critical-flux conditions, because there is little or no creation of unstable modes during growth. The interfacial kinetics have a strong stabilizing effect, which was explored in detail here.

This work has important implications for shape control in processing applications; shape control may be achieved by varying the undercooling in time to approximate near-critical flux conditions. Experiments are currently being designed (by Stefano Guido and coworkers [4] at the University of Naples) to test this possibility.

In Part II [5] of our study, we will investigate the nonlinear evolution using adaptive boundary-integral simulations, in which the number of marker points N of the computational mesh is changed during a simulation to resolve the interface $\Sigma(t)$ to a prescribed accuracy. This enables us to simulate three dimensional crystals stably and accurately well into the nonlinear regime. Preliminary results indicate that this class of solutions is robust with respect to perturbations and is well-predicted by solutions of the linearized equations. Simulations of both stable and unstable crystal growth will be presented. An example is given in figure 4, for the case of unstable growth and constant far-field temperature T^{∞}. From figure 1 and formula (3.10), the generation of an increasing number of unstable modes is evident during the evolution: there is no unstable mode at $t = 0$, whereas there are ≈ 16 unstable modes corresponding to the last frame in figure 4 (the maximum growth rate occurs for mode ≈ 10).

In the physical system, typically both surface tension γ and kinetic coefficient μ are anisotropic [13]. This introduces preferred directions of growth, where surface tension (or kinetics) is minimum, leading to the formation of dendrites, travelling waves, and to non-trivial stationary shapes and the possibility for self-similar growth. Extension of the linear theory and the boundary-integral method to include anisotropies in 3-D is underway.

ACKNOWLEDGMENTS

VC and JL acknowledge partial support from the National Science Foundation, the Institute of Mathematics and its Applications for their hospitality, the Minnesota Supercomputing Institute for computer time, and Professor P. Leo from the University of Minnesota for discussions. VC also acknowledges a Research Scholarship from the Minnesota Supercomputing Institute.

REFERENCES

[1] W. Mullins and R. Sekerka, J. Appl. Phys. **34**, 323 (1963).

[2] S.R. Coriell and R.L. Parker, J. Appl. Phys. **36**, 632 (1965).

[3] S.R. Coriell and R.L. Parker, in: Crystal Growth, Ed. H. S. Peiser (Pergamon, Oxford, 1967) 703.

[4] M. Simeone and S. Guido, Personal communication.

[5] V. Cristini and J. Lowengrub, In preparation.

[6] J. M. Ball, D. Kinderlehrer, P. Podio-Guidugli, M. Slemrod (Eds.), Evolving phase interfaces in solids, Springer, New York, 1999.

[7] V. Cristini, J. Lowengrub and Q. Nie, J. Math. Biol., In review.

[8] T. Y. Hou, J.S. Lowengrub and M. J. Shelley, J. Comp. Phys. **114**, 312 (1994).

[9] H.-J. Jou, P. H. Leo and J.S. Lowengrub, J. Comp. Phys. **131**, 109 (1997).

[10] J. W. Cahn, W. B. Hillig and G. W. Sears, Acta Met. **12**, 1421 (1964).

[11] I. M. Lifshitz and V. V. Slyozov, J. Phys. Chem. Solids **19**, 35 (1961).

[12] C. Wagner, Z. Elektrochem **65**, 581 (1961).

[13] S. R. Coriell and R. F. Sekerka, J. Crystal Growth **34**, 157 (1976).

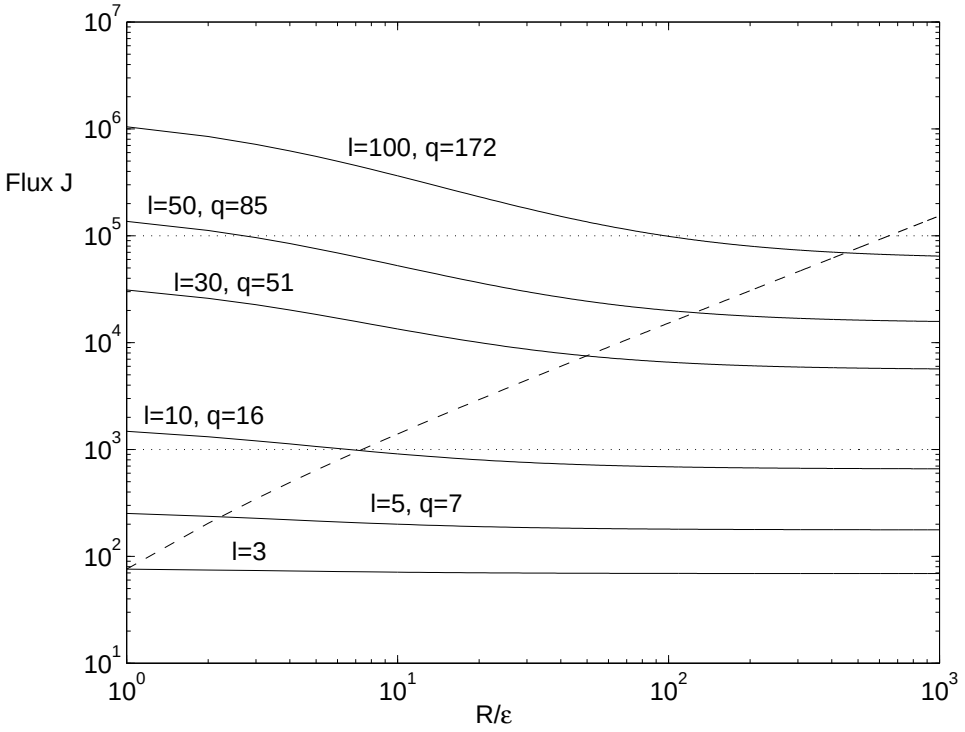

FIG. 1. Flux J from Eq. (3.10) versus R/ϵ (solid) when l is the unstable mode with largest growth rate $(\delta/R)^{-1}\frac{\mathrm{d}}{\mathrm{d}t}(\delta/R)$; $k = 1$. Correspondingly, q marks the upper bound of the band of unstable modes. Evolutions are also shown with J constant (dotted) and T^{∞} constant (dashed, where the flux is obtained from Eq. (3.4)).

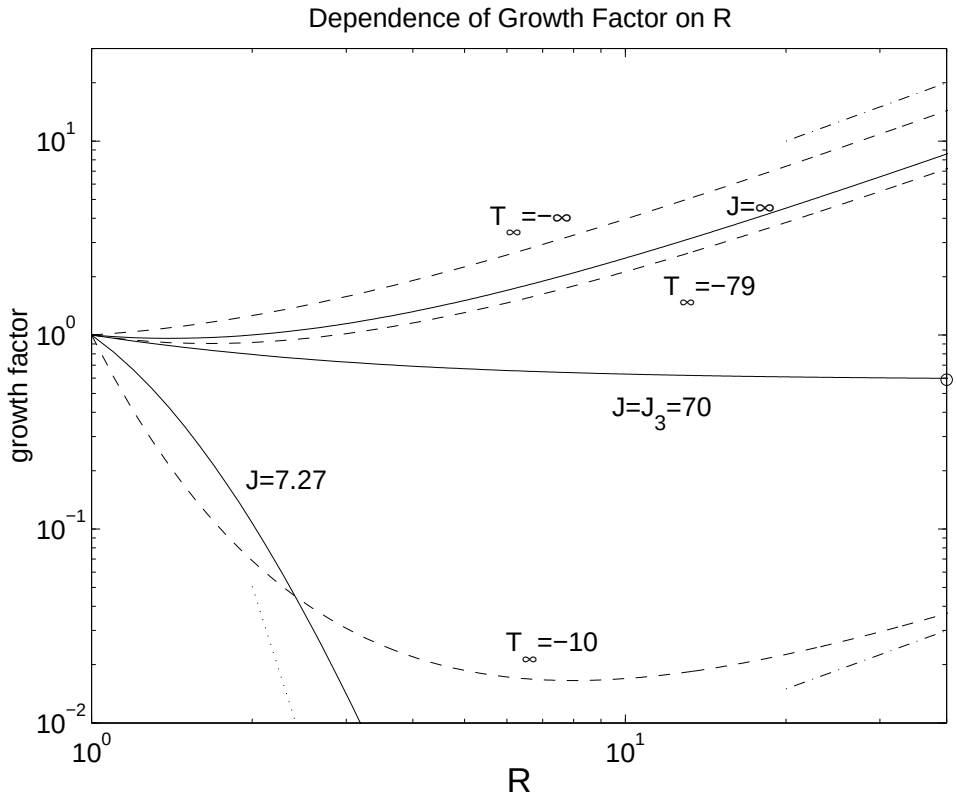

FIG. 2. Growth factor $(\delta/\delta_0)/R$ as a function of R for $l = 3$, $k = 1$, $\epsilon = 0.1$. The solid and dashed curves correspond to constant J and T^∞ as labeled. At time $t = 0$, the J and T^∞ are related by the formula (3.4): $J = 7.27$ corresponds to $T^\infty = -10$, $J = 70$ to $T^\infty = -79$, and $J = \infty$ to $T^\infty = -\infty$. The open circle is the limiting value for $J = J_3$. The dotted line has the limiting slope for $J = 7.27$ and the dot-dashed lines are the limiting slopes for $J \to \infty$ and for T^∞ constant, as $R \to \infty$.

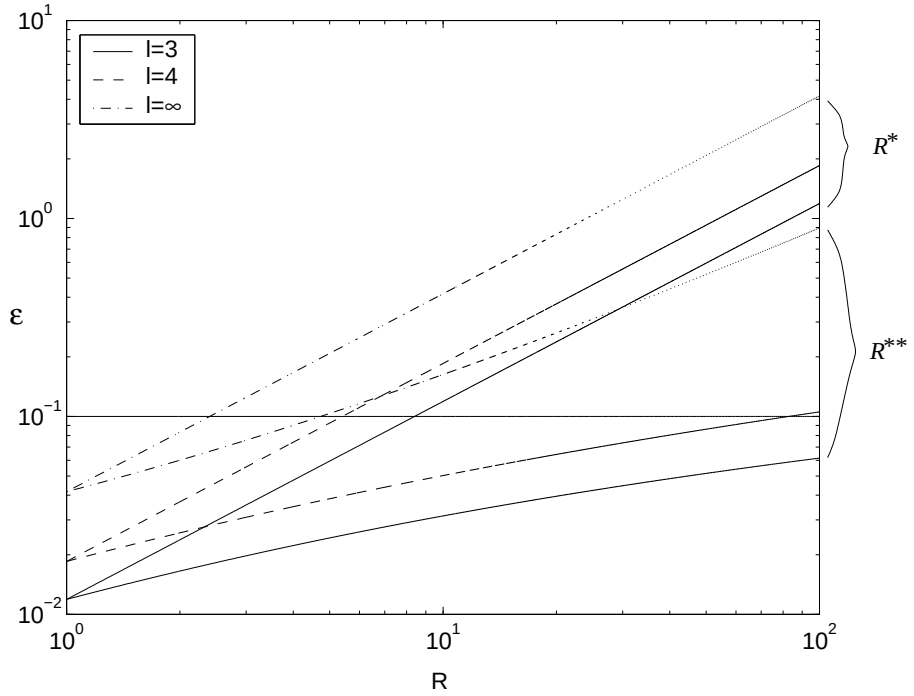

FIG. 3. Dimensionless kinetic coefficient ϵ as a function of R_l^* and R_l^{**}, from Eqs. (3.20)–(3.21); $l = 3$, 4 and ∞; $k = 1$. In each case, $J = 1.1J_l$. The horizontal line marks the value $\epsilon = 0.1$.

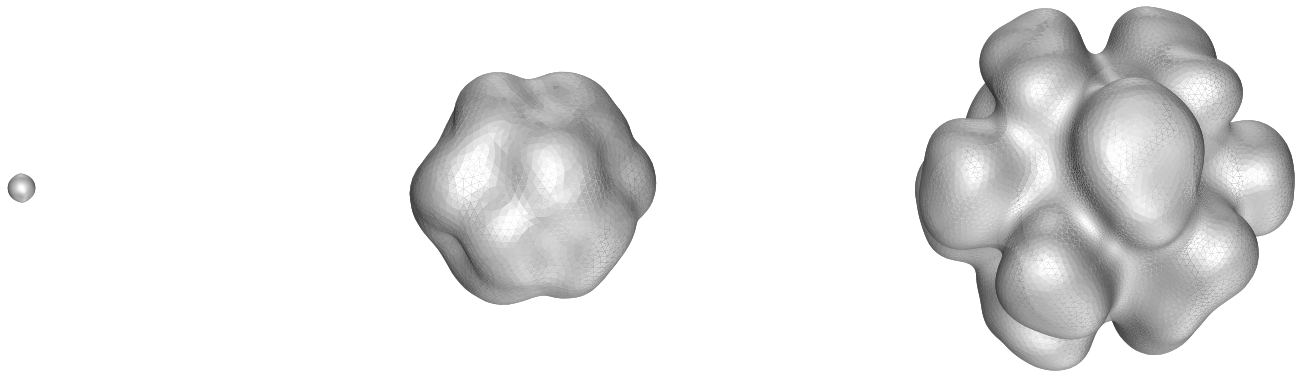

FIG. 4. Adaptive 3-D boundary-integral simulation of unstable growth with constant far-field temperature $T^\infty = -60$; initial shape $r_{\Sigma,0} = 1 + \delta_0^{3,0}\, Y_{3,0} + \delta_0^{4,0}\, Y_{4,0} + \delta_0^{4,3}\, Y_{4,3} + \delta_0^{5,5}\, Y_{5,5} + \delta_0^{6,6}\, Y_{6,6} + \delta_0^{10,6}\, Y_{10,6} + \delta_0^{12,2}\, Y_{12,2}$, where $\delta_0^{3,0} = 6.7 \cdot 10^{-7}$, $\delta_0^{4,0} = 5 \cdot 10^{-4}$, $\delta_0^{4,3} = 5 \cdot 10^{-7}$, $\delta_0^{5,5} = 4 \cdot 10^{-4}$, $\delta_0^{6,6} = 0.002$, $\delta_0^{10,6} = 0.001$, $\delta_0^{12,2} = 5 \cdot 10^{-4}$; $\epsilon = 0.1$, $k = 1$. Configurations are shown at times $t = 0$ ($R = 1$, $J = 54.5$, $N = 1,068$), $t = 0.605$ ($R = 8.24$, $J = 502$, $N = 3,800$), $t = 1.115$ ($R = 11.73$, $J = 744$, $N = 19,864$). The computational mesh is not shown.